Supplementary Figure 1.

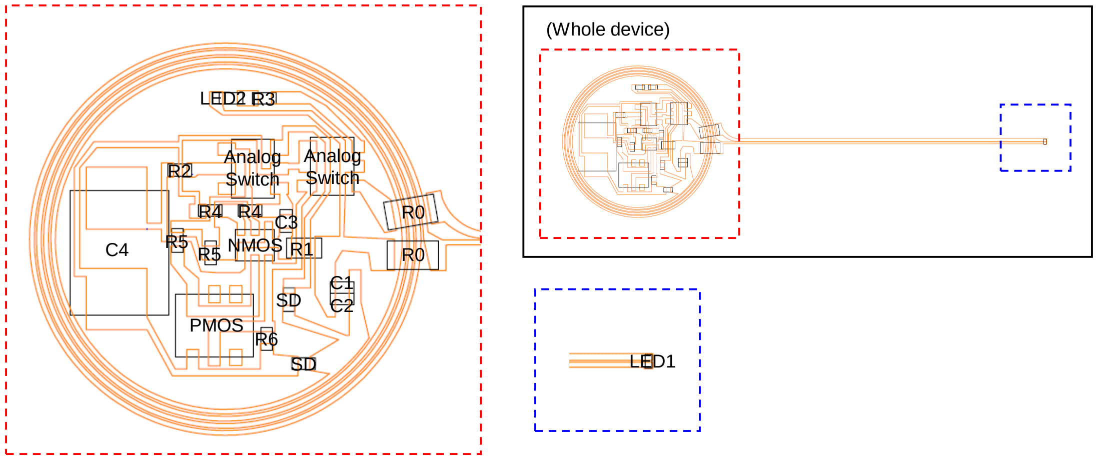

	Components	Product number	Vendor information
LED1	460nm, 220 µm x 270 µm x 50 µm	C460TR2227	Cree
LED2	632nm, 0.65 mm x 0.35 mm x 0.2 mm	APG0603SEC-E-TT	Kingbright
SD	Schottky Diode, 0.65 mm x 0.35 mm x 0.3 mm	DSR01S30SL	Toshiba
R0	0 ohm, 1.6 mm x 0.9 mm x 0.55 mm	RCWPM-0603	VISHAY
R1	0 ohm, 1.00 mm x 0.55 mm x 0.35 mm	RCWPM-0402	VISHAY
R2	0 ohm, 0.65 mm x 0.35 mm x 0.25 mm	RCWPM-0201	VISHAY
R3	499 ohm, 0.6 mm x 0.3 mm x 0.23 mm	RC0603F4990CS	Samsung Electro-Mechanics
R4	249 kohm, 0.6 mm x 0.3 mm x 0.23 mm	RC0603F2493CS	Samsung Electro-Mechanics
R5	10 kohm, 0.6 mm x 0.3 mm x 0.23 mm	RC0603J103CS	Samsung Electro-Mechanics
R6	20 kohm, 0.6 mm x 0.3 mm x 0.23 mm	RC0603F203CS	Samsung Electro-Mechanics
C1	82 pF, 0.6 mm x 0.3 mm x 0.33 mm	CL03C820JA3NNNC	Samsung Electro-Mechanics
C2	330 pF, 0.6 mm x 0.3 mm x 0.33 mm	CL03B331KA3NNNC	Samsung Electro-Mechanics
C3	1 µF, 0.6 mm x 0.3 mm x 0.33 mm	CL03A105KP3NSNC	Samsung Electro-Mechanics
C4	11 mF, 3.2 mm x 2.5 mm x 0.9 mm	CPH3225A	Seiko Instruments
NMOS	1.0 mm x 1.0 mm x 0.34 mm	NTUD3170NZ	ON Semiconductor
PMOS	1.7 mm x 1.7 mm x 0.6 mm	NX3008PBKV	Nexperia
Analog Switch	1.6 mm x 1.2 mm x 0.5 mm	SN74LVC1G3157	Texas Instruments

Supplementary Figure 1. Device layout (top) and a table of components used for the wireless gastric optogenetic implant (bottom).

Supplementary Figure 2.

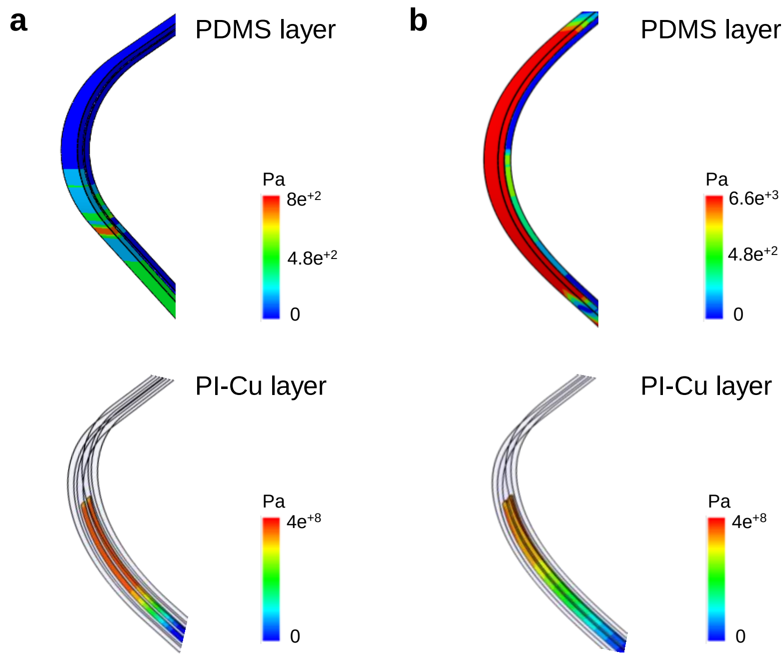

Supplementary Figure 2. Three dimensional modeling of the mechanics for the pre-curved (**a**) and post-curved (**b**) structure.

Supplementary Figure 3.

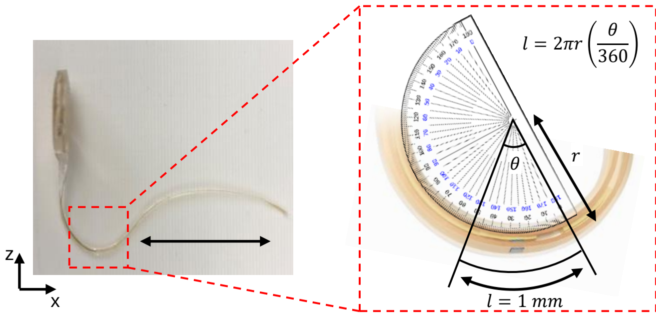

Supplementary Figure 3. Measurement method and equation for various curvatures of a tether.

Supplementary Figure 4.

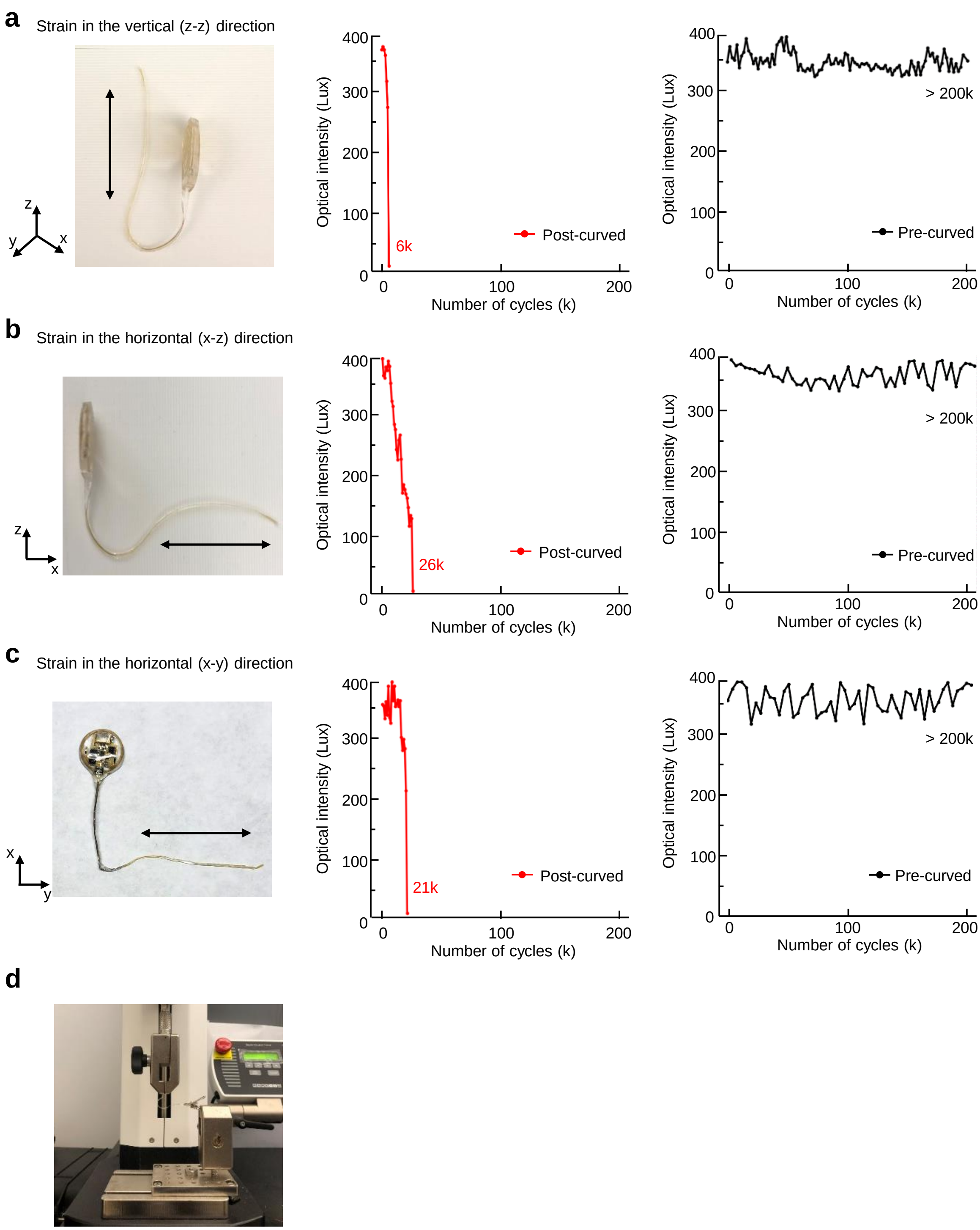

Supplementary Figure 4. Image of a device (left) and results of cycling test for the post-curved (middle) & pre-curved structure (right) when strains applied in the z (**a**), x (**b**), and y (**c**) direction, respectively. Here, an arrow indicate the direction of strains applied to the device. (**d**) Measurement setup for durability test.

Supplementary Figure 5.

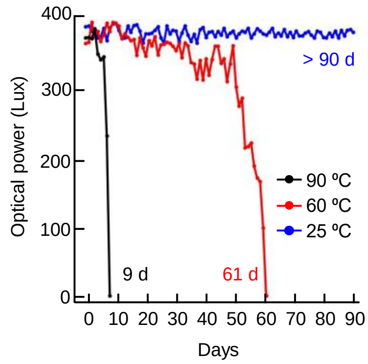

Supplementary Figure 5. Measurements of optical output power from devices when immersed in saline solution at various temperatures, 25 °C, 60 °C & 90 °C.

Supplementary Figure 6.

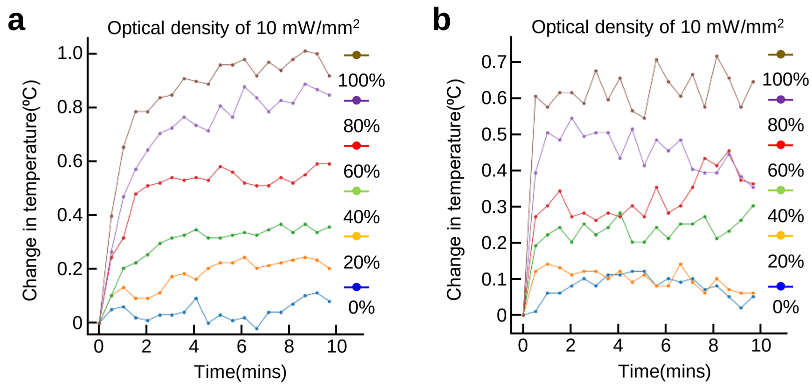

Supplementary Figure 6. Measurements of temperature changes as a function of operation duty cycles in wet (**a**) and dry condition (**b**).

Supplementary Figure 7.

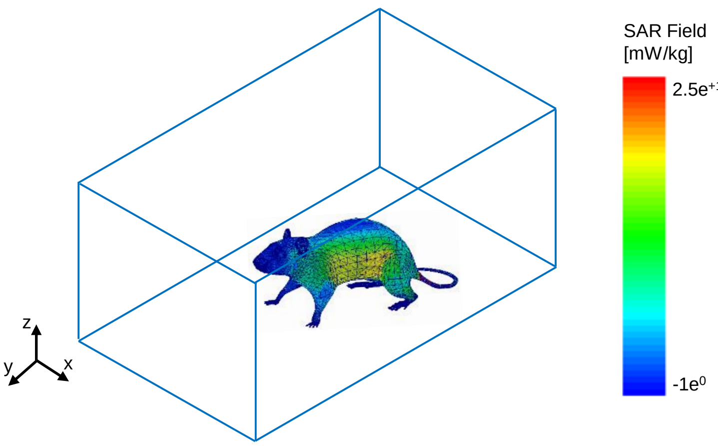

Supplementary Figure 7. An experimental assay with computed SAR distributions on a mouse mesh body.

Supplementary Figure 8.

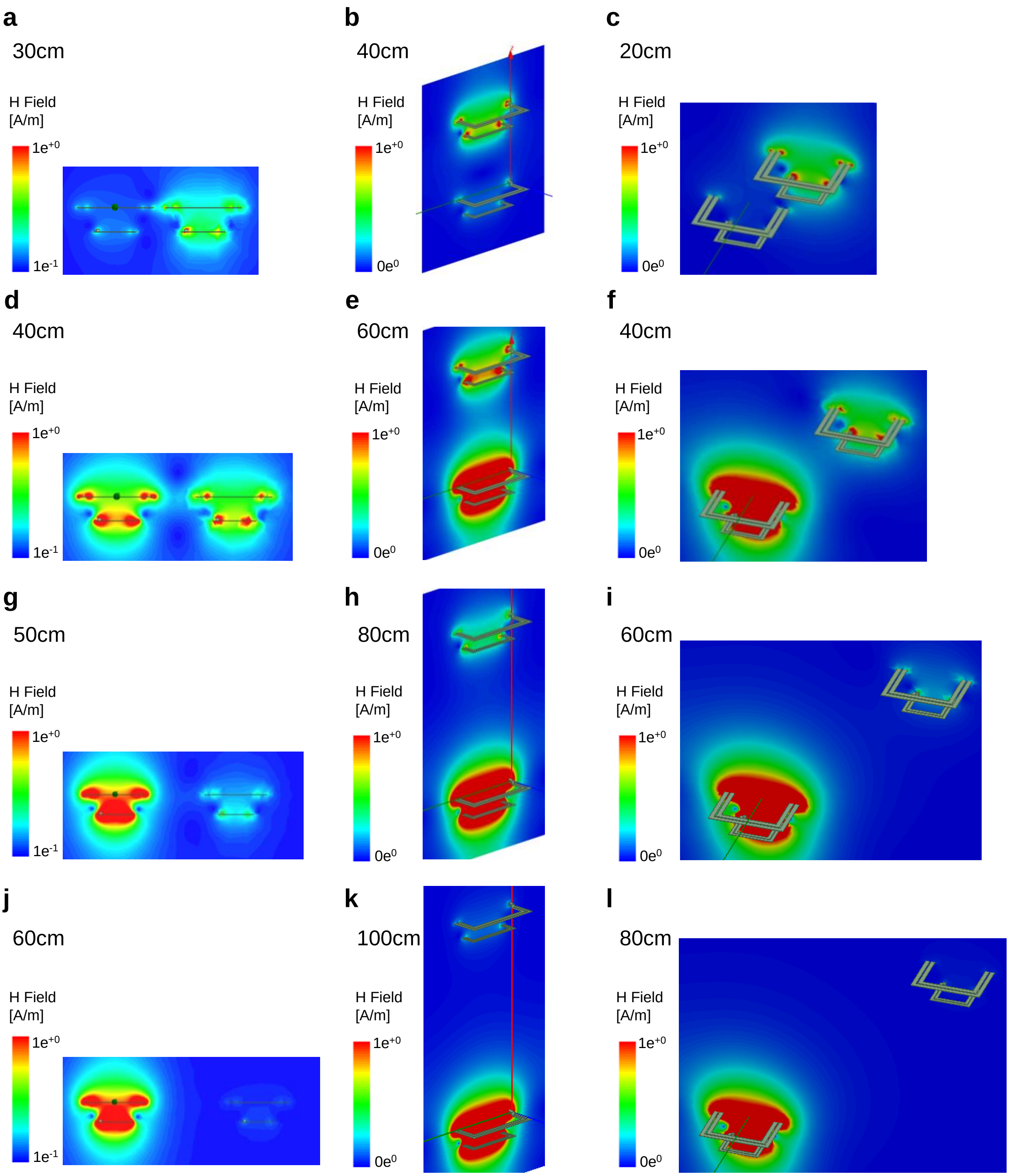

Supplementary Figure 8. Simulation results of electromagnetic couplings induced in an adjacent cage as a function of distance between two cages along the horizontal (**a-d**), vertical (**e-g**), and diagonal (**i-l**) direction, respectively at a transmitted power level of 4 W.

Supplementary Figure 9.

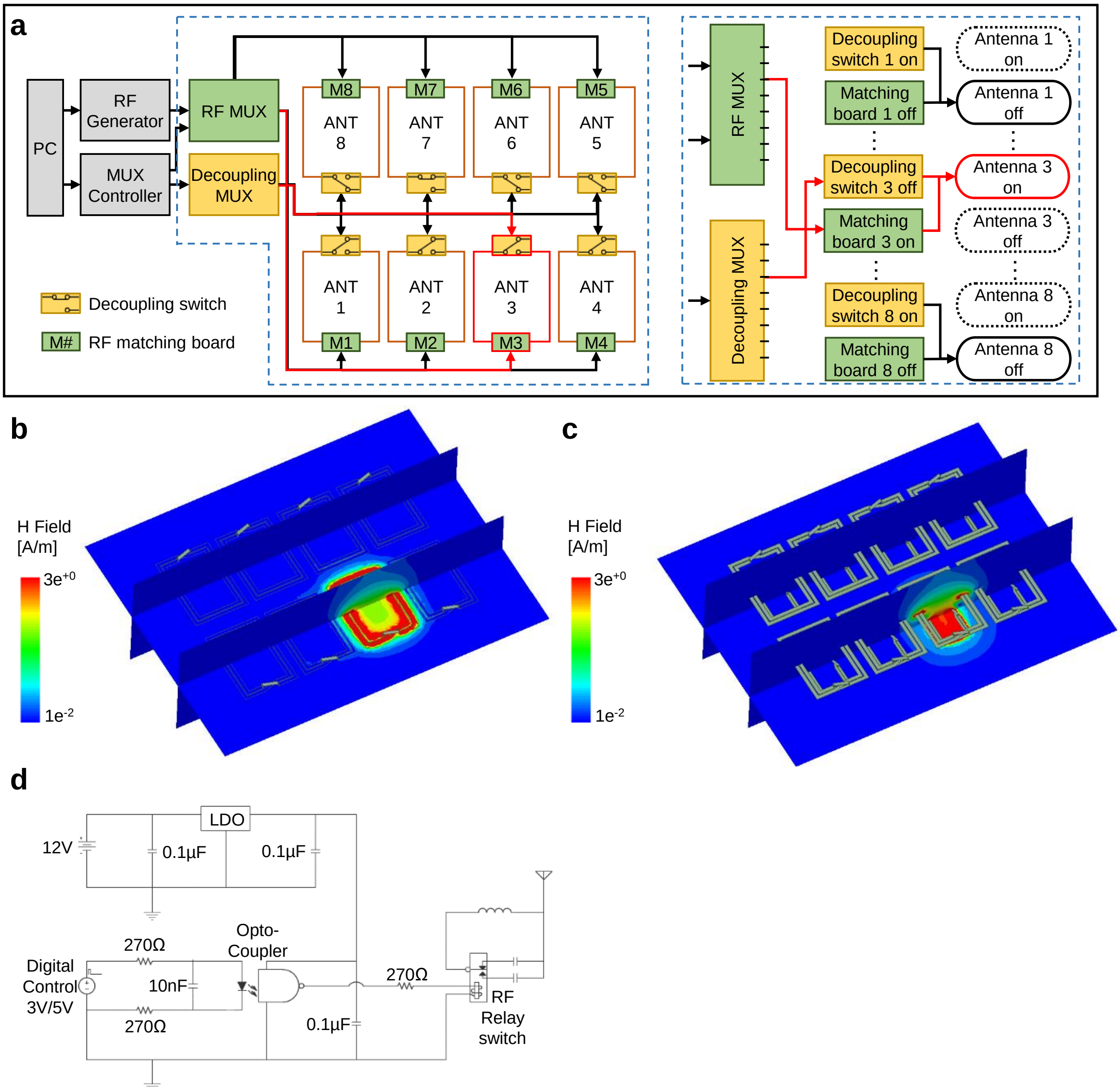

Supplementary Figure 9. (**a**) Functional block diagram of the proposed 1 × 8 multiple cage wireless power transmission system. Distributions of electromagnetic field on the top antenna coil (**b**) and the bottom antenna coil (**c**) at a transmitted power level of 4W. (**d**) Circuit diagram of decoupling MUX.

Supplementary Figure 10.

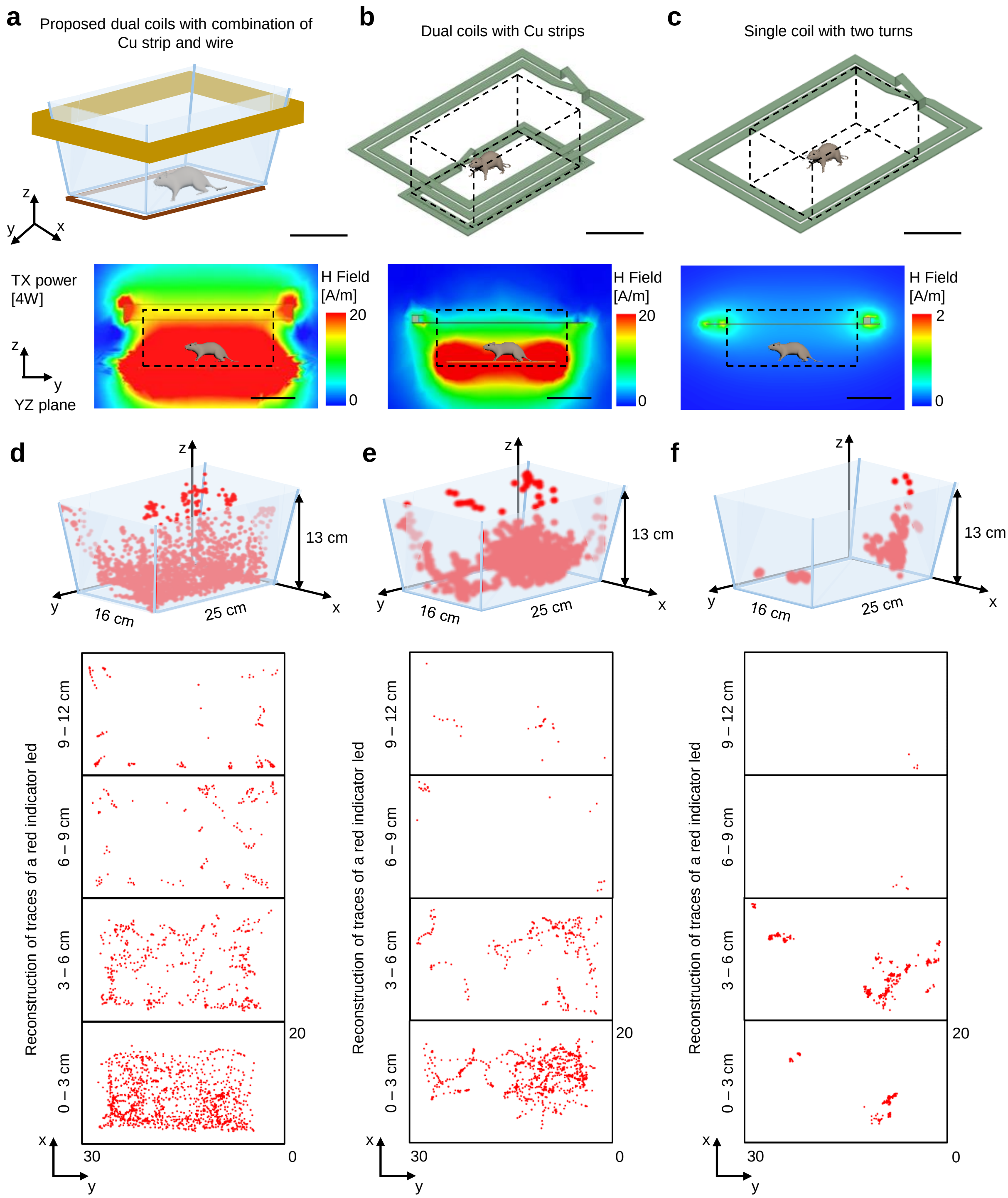

Supplementary Figure 10. Illustration of an antenna layout (top) and distributions of magnetic field in a cage (bottom) for the proposed (**a**), dual coil with Cu strips (**b**), and single coil antenna structure (**c**), respectively; scale bar 10 cm. Reconstruction of traces of an operating indicator led (top) and cross-sectional view of it at each ranges of height for the proposed (**d**), dual coil with Cu strips (**e**), and single coil antenna structure (**f**), respectively.

Supplementary Figure 11.

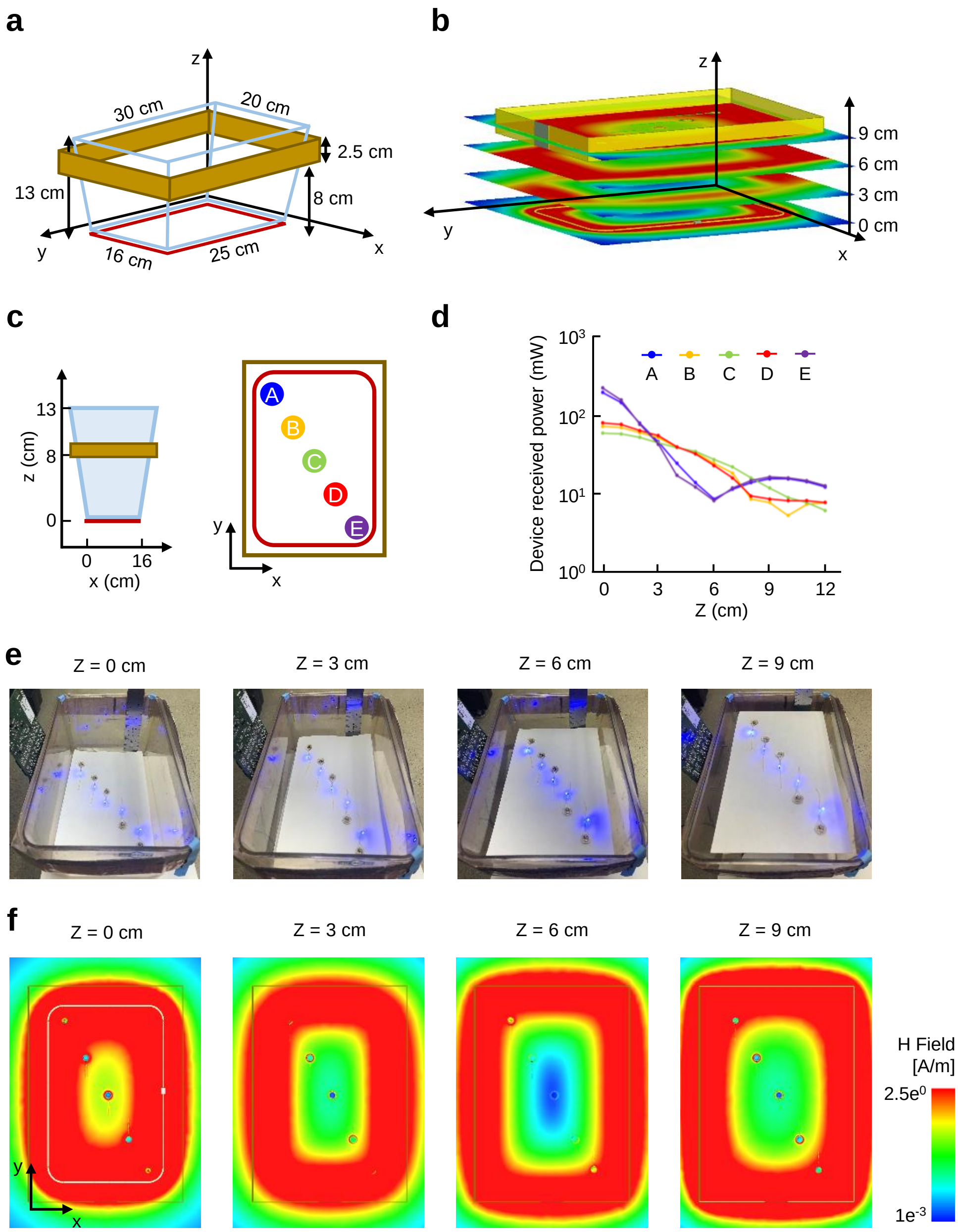

Supplementary Figure 11. (**a**) Representative image of a cage with the proposed antenna coils installed. (**b**) Distributions of electromagnetic field in a cage at each distances from the bottom. (**c**) Illustration of measurement setup. (**d**) Measurements of output power at 5 different locations of the cage as a function of the distance along the z axis. (**e**) Representative images of wireless operation in the cage at each distance. (**f**) Corresponding distributions of electromagnetic field in the cage at each distance from the bottom.

Supplementary Figure 12.

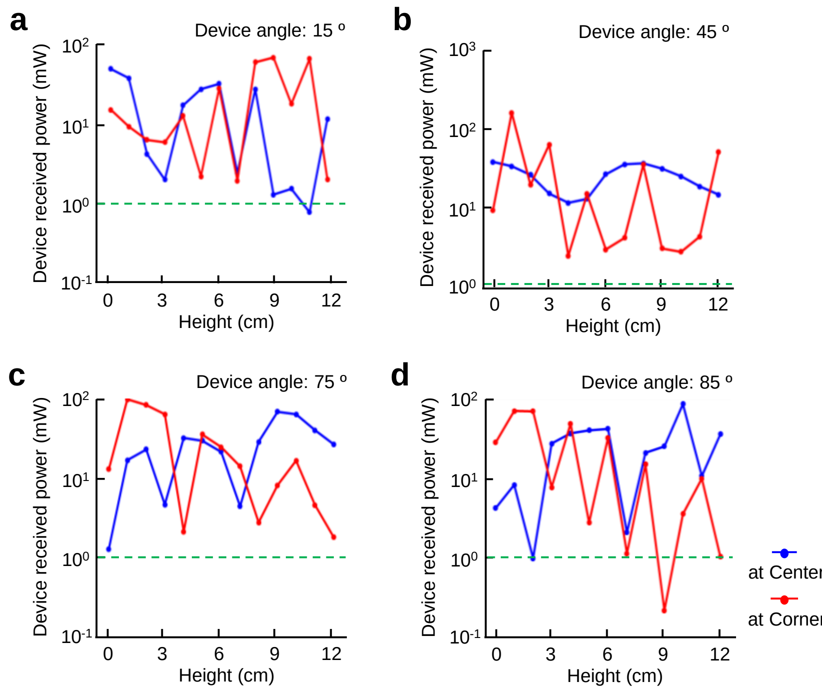

Supplementary Figure 12. Plots of a residual dependence of transmitted power on relative orientation angle between the transmission antenna and the implantable device as a function of the angle, 15 º (**a**), 45 º (**b**), 75 º (**c**), and 85 º (**d**). Green dotted lines indicate indicate threshold electrical power level of 1 mW required for activation of light-sensitive proteins; 1mW electrical power corresponding to an optical power of 17.44 mW/mm^2.

Supplementary Figure 13.

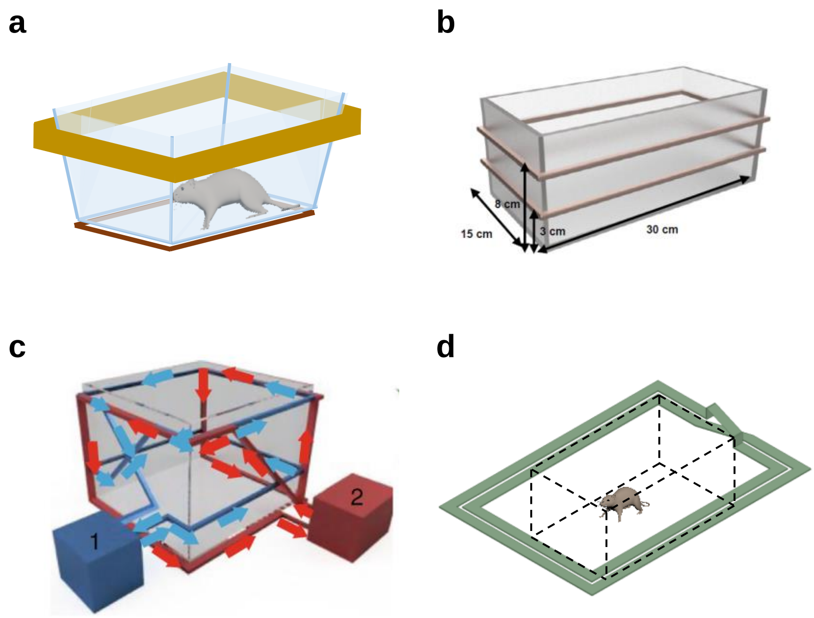

Supplementary Figure 13. Comparison of wireless coverage for the proposed antenna coil and other antenna coil systems. Representative image of the proposed antenna coil (**a**), single coil & dual layered with Cu wire (**b**), a tilted antenna design with a time division multiplexing scheme (**c**), dual coil antenna with Cu strips, and single coil with two turns (**d**).

Supplementary Figure 14.

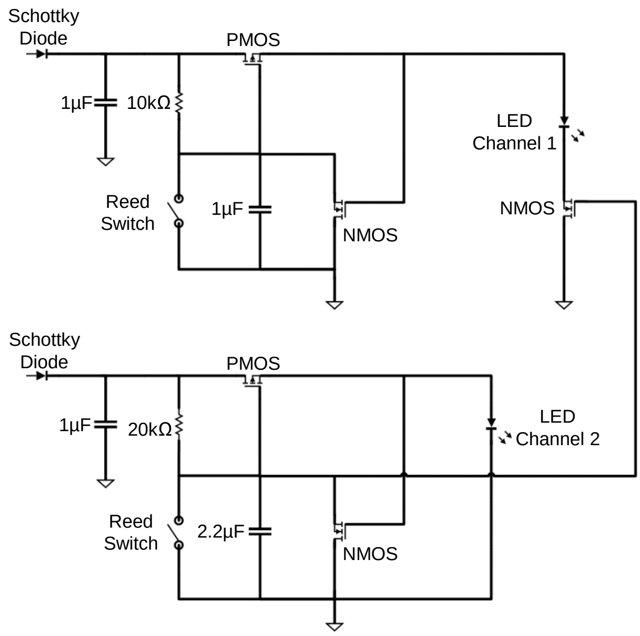

Supplementary Figure 14. Circuit diagram of the proposed, scalable multimodal wireless gastric optogenetic implant for multiple organ control.

Supplementary Figure 15.

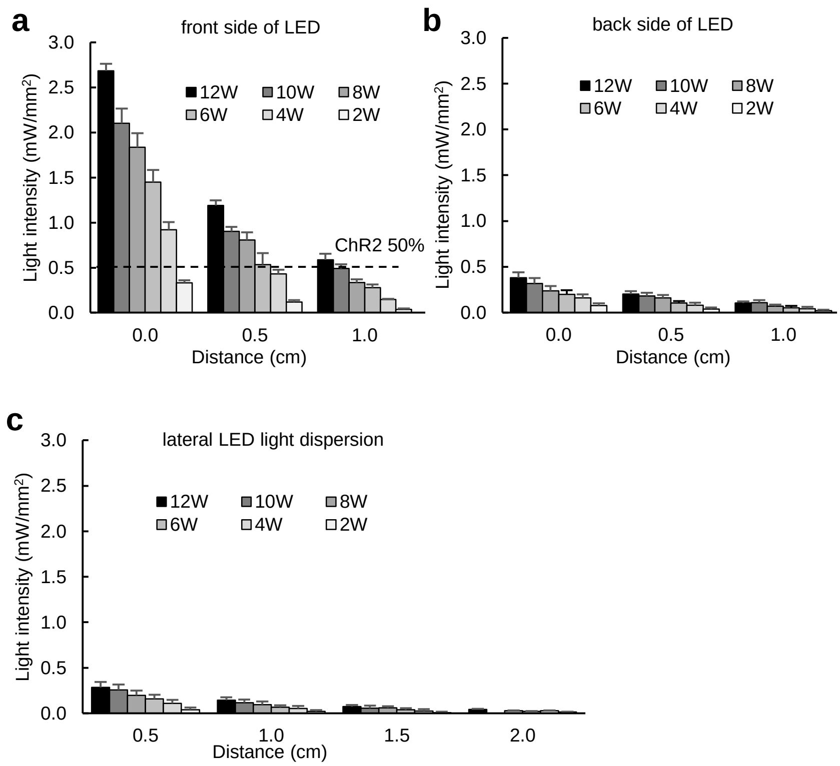

Supplementary Figure 15. Light intensity measurements during varying RF wireless powering of the gastric optogenetic device (n = 5) and varying distances from the LED. Measurements were taken from the front side (**a**), back side (**b**), and lateral side of the LED (**c**). Bar graphs are mean ± SEM.

Supplementary Figure 16.

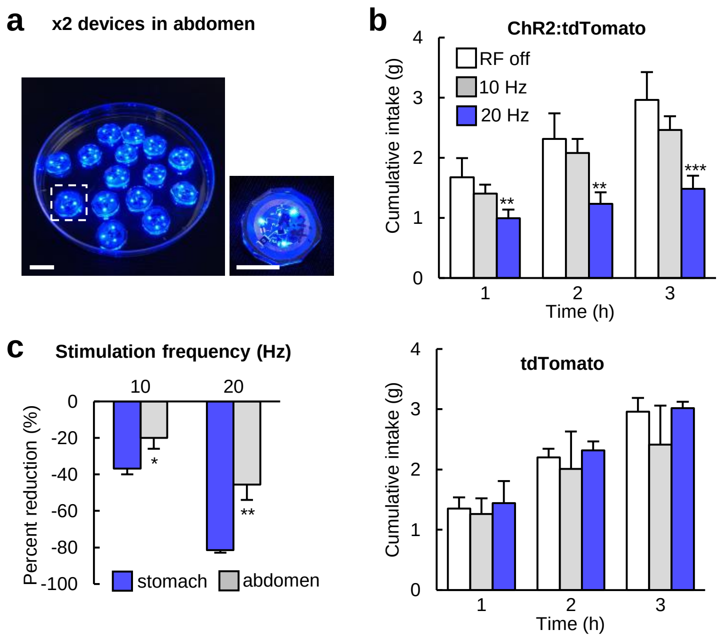

Supplementary Figure 16. Abdominal activation of *Calca*+ vagal afferent fibers. (**a**) Picture showing wirelessly powered LED device; two of these devices were inserted into the abdomen of *Calca*-Cre transgenic mice with left nodose ganglion injection of AAV9-DIO-ChR2:tdTomato or AAV9-DIO-tdTomato control virus; scale bar 5 mm. (**b**) top, frequency dependent suppression of food intake during ChR2 activation of vagal afferents (n = 8), bottom, no appetite suppression in tdTomato control group (n = 4). (**c**) Percent reduction of food intake (compared to RF off) during 10 and 20 Hz stimulation of *Calca*+ vagal afferent endings using the stomach LED implant or non attached LEDs (ChR2, n = 8 per group). Bar graphs are mean ± SEM. * $p < 0.05$; ** $p < 0.01$; *** $p < 0.001$.

Supplementary Figure 17.

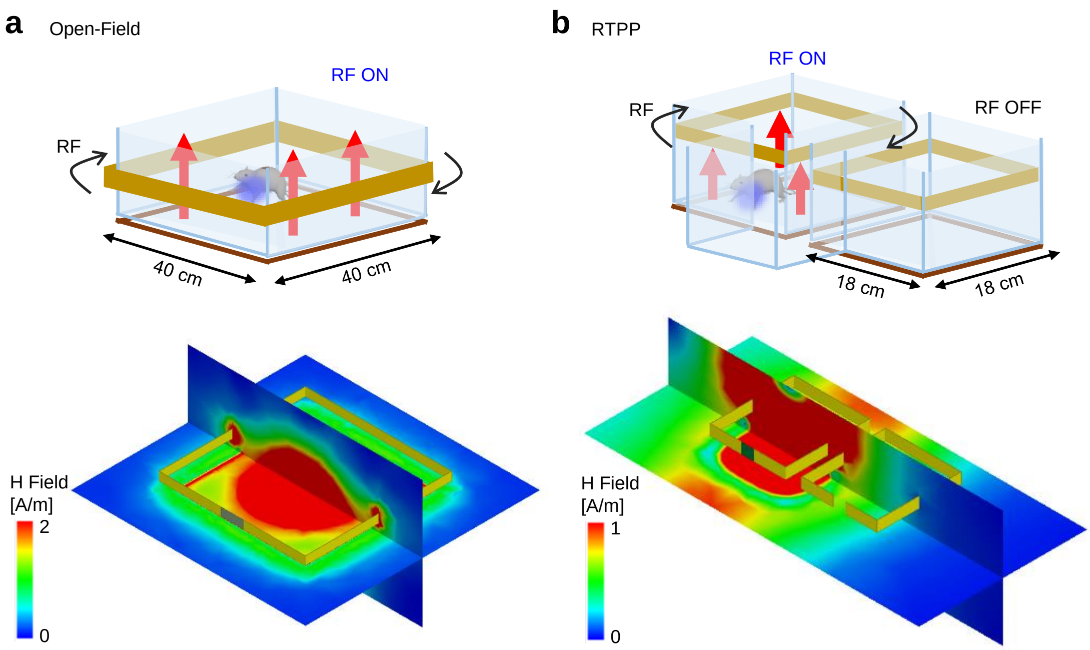

Supplementary Figure 17. Schematic illustration of an experimental assay (top) and distributions of electromagnetic field in the assay (bottom) for open-field (**a**) and RTPP (**b**), respectively.